Influence of Indenter Tip Geometry on Elastic Deformation during Nanoindentation

H. Bei,[1,2] E. P. George,[1,2] J. L. Hay,[3] and G. M. Pharr[1,2]

[1]*Department of Materials Science and Engineering, The University of Tennessee, Knoxville, Tennessee 37996, USA*
[2]*Metals and Ceramics Division, Oak Ridge National Laboratory, Oak Ridge, Tennessee 37831, USA*
[3]*Nano Instruments Innovation Center, MTS Systems Corporation, Oak Ridge, Tennessee 37830, USA*

(Received 28 January 2005; published 19 July 2005)

Nanoindentation with a Berkovich indenter is commonly used to investigate the mechanical behavior of small volumes of materials. To date, most investigators have made the simplifying assumption that the tip is spherical. In reality, indenter tips are much more complex. Here, we develop a new method to describe the tip shape using the experimentally determined area function of the indenter at small depths (0–100 nm). Our analysis accurately predicts the elastic load-displacement curve and allows the theoretical strength of a material to be determined from pop-in data. Application of our new method to single crystal Cr_3Si shows that the predicted theoretical strengths are within 12% of the ideal strength $G/2\pi$, where G is the shear modulus.

DOI: 10.1103/PhysRevLett.95.045501 PACS numbers: 62.25.+g, 62.20.Dc, 62.20.Fe, 81.07.Lk

Nanoindentation is a useful technique for measuring the mechanical properties of small volumes of materials [1]. Often it is performed with a Berkovich indenter which has the shape of a three-sided pyramid with triangular faces. Real Berkovich indenters are not perfectly sharp but are blunt to varying degrees. The most common approximation that has been used to describe a blunt Berkovich indenter is that it is spherical near the tip. However, the radius, R, of such a spherical tip is not well known. Some investigators have used tip radii quoted by manufacturers [2–4], but these are subject to great uncertainty since they are usually no more than order-of-magnitude estimates, in addition to which the actual radius may change during use due to wear. To circumvent this problem, others have attempted to directly measure the tip radius by atomic force or scanning electron microscopy [5,6]. Another popular approach is to fit the elastic load-displacement data by the Hertzian relation:

$$P = \frac{4}{3} E_r R^{1/2} h^{3/2}, \tag{1}$$

where P is the indenter load, h is its displacement, and E_r is a reduced elastic modulus [7]. Once the radius is known, the stresses in the material can be evaluated from Hertzian contact mechanics as a function of the applied load.

Although a reasonable first approach, the tips of most Berkovich indenters are not truly spherical over the range of depths at which most measurements are made. In this Letter, rather than assuming a spherical tip, we describe the geometry using the area function measured in the indenter tip shape calibration procedure and examine the influence this has on one aspect of nanoscale mechanical behavior, namely, the theoretical strengths calculated from pop-in data. Pop-in events are characterized by sudden bursts of displacements at specific indentation loads which produce discontinuous steps in otherwise smooth load-displacement curves. They have been investigated during nanoindentation with pyramidal and spherical indenters in crystalline [1–6,8–12] and amorphous materials [13,14]. In crystalline materials devoid of surface oxides and other contaminating surface layers, the first pop-in event signifies the transition from purely elastic to elastic/plastic deformation and is thought to be associated with the nucleation of dislocations [2–6,8–12]. Since the first extensive study of pop-in events in sapphire by Page *et al.* [9], it has been observed in numerous metals and ceramics, particularly those in which the initial dislocation density is low and/or the mobility of existing dislocations is severely restricted. The shear strength at pop-in events is frequently close to the theoretical strength $G/2\pi$, where G is the shear modulus. The depths at which pop-in events have been observed range from ~6–120 nm [1–6,8–12].

We report here results of nanoindentation experiments carried out with a diamond Berkovich indenter on a Cr_3Si single crystal grown as described elsewhere [15]. Finite element analyses, using the Virtual Indenter™ finite element simulation package (MTS Corporation, Knoxville, TN), were used to determine the maximum resolved shear stresses at the pop-in load from the measured indenter shape and compared to analyses assuming a spherical tip to establish important differences.

A large and reproducible pop-in event was observed in the Cr_3Si single crystals, an example of which is shown in Fig. 1. The magnitude of the pop-in load varied with crystallographic orientation, presumably due to differences in the shear stress resolved onto the slip system. Cr_3Si has the $A15$ crystal structure and slips on (100)[001]. The average pop-in loads based on 10 measurements for each of the three low-index orientations were as follows: 5.4 ± 0.4 mN for [100]; 3.9 ± 0.3 mN for [110]; 4.7 ± 0.4 mN for [111]. The pop-in loads and displacements are summarized in Table I.

The area function of the indenter was determined over the depth range 0–100 nm by performing experiments in fused quartz, which is the standard calibration material. This particular range was chosen to give accurate measure-

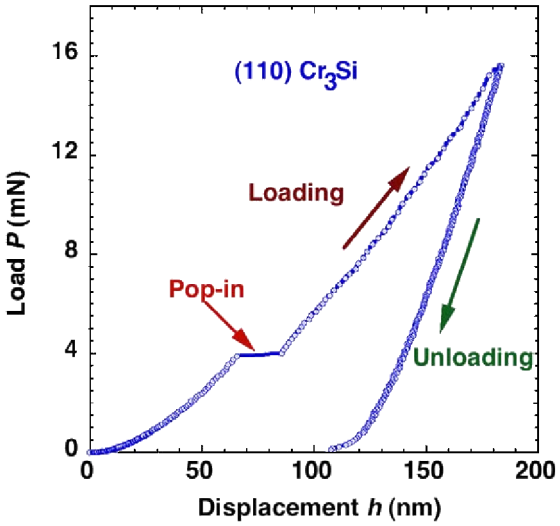

FIG. 1 (color online). Load-displacement data for a (110) single crystal of Cr_3Si illustrating the pop-in behavior.

ments at the depths at which a pop-in event was observed (61–83 nm; see Table I). The area function was measured using a minor variation on the Oliver-Pharr method. The contact depths, h_c, were evaluated using exactly the procedures developed by Oliver and Pharr, but the contact areas, A, were determined from the dynamically measured contact stiffnesses, S, by means of the contact stiffness/area relation [16]:

$$A = \frac{\pi}{4}\left(\frac{S}{\beta E_r}\right)^2. \tag{2}$$

The constants used to evaluate this expression were $E_r = 69.6$ GPa based on the elastic constants of fused quartz and diamond indenter, and $\beta = 1.034$ (the normally assumed value) [1]. The area function so determined is shown as the experimental data points in Fig. 2. Using standard curve-fitting procedures, the A vs h_c data in Fig. 2 were found to be well described by the simple two-parameter relation:

$$A = \alpha_1 h_c^2 + \alpha_2 h_c, \tag{3}$$

where $\alpha_1 = 25.97$ and $\alpha_2 = 1457$ (h_c is in units of nm; A in units of nm^2). The form of this relation, which we have observed to work well for many Berkovich indenters, has a simple physical interpretation. The first term represents a conical or pyramidal indenter ($\alpha_1 = 24.56$ for a perfect Berkovich indenter). The second term describes a spherical indenter in the limit $h_c \ll R$. This follows from the exact relation for a sphere,

$$A = 2\pi R h_c - \pi h_c^2, \tag{4}$$

which reduces to $A = 2\pi R h_c$ when $h_c \ll R$. Consequently, $\alpha_2 = 2\pi R$, meaning that the sphere for which $\alpha_2 = 1457$ has a radius $R = 232$ nm. Because of the different dependencies on h_c, the conical first term in Eq. (3) dominates at large penetration depths, while the spherical second term is more important at small depths. Equation (3) thus provides a natural way to interpolate between the two important limiting cases of spherical contact at small depths and conical or pyramidal contact at large depths. The cone for which $\alpha_1 = 25.97$ has a semivertical angle of 70.8° rather than 70.3°, which is the conical equivalent of a perfect Berkovich indenter.

The relative contributions of the individual terms to the contact area are plotted along with the experimental data in Fig. 2. Note that, in the depth range of interest for the analysis of the pop-in data, neither term is dominant, and the contributions of both must be considered to obtain the correct contact areas. For this reason, analyses based strictly on the spherical tip assumption can lead to errors.

Assuming that the indenter is axially symmetric, the relation between the contact radius, a, and the contact depth, h_c, derived from Eq. (3) is

$$a^2 = \frac{\alpha_1}{\pi} h_c^2 + \frac{\alpha_2}{\pi} h_c = C_1 h_c^2 + C_2 h_c, \tag{5}$$

where $C_1 = \alpha_1/\pi$ and $C_2 = \alpha_2/\pi$. In r-z cylindrical coordinates, the shape of the axially symmetric indenter is then given by

$$z = f(r/a) = \frac{-C_2 + \sqrt{C_2^2 + 4C_1(r/a)^2}}{2C_1}. \tag{6}$$

We will use this function to describe the indenter tip shape in all subsequent analyses.

Since the indenter shape described by Eq. (6) is smooth (i.e., infinitely differentiable) and $f(0) = 0$, an analytical method developed by Sneddon [17] can be used to deter-

TABLE I. Measured and computed parameters for Cr_3Si single crystals.

Indentation direction	[100]	[110]	[111]
Load at pop-in event, P (mN)	5.4 ± 0.4	3.9 ± 0.3	4.7 ± 0.4
Displacement at pop-in event, h (nm)	83	61	74
Contact radius at pop-in event, a (nm)	197	158	184
Effective sphere radius, R_{eff} (nm)[a]	412	379	358
Maximum τ_R (finite element analysis) (GPa)	18.1	22.3	21.7
Maximum τ_R (Hertz $R = 232$ nm) (GPa)	23.9	31.4	26.4
Maximum τ_R (Hertz $R = R_{\text{eff}}$) (GPa)	16.4	22.7	19.6

[a]Based on Hertzian analysis.

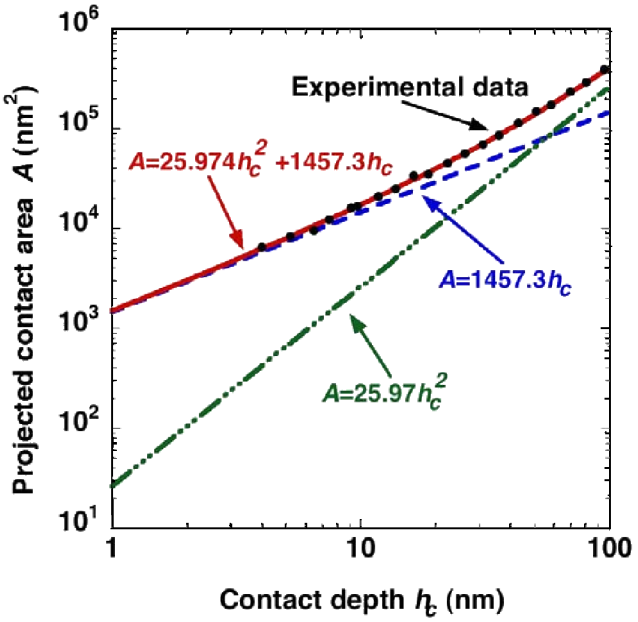

FIG. 2 (color online). Measured area function for the Berkovich indenter at depths up to 100 nm (circles) compared to the area function used in our calculations.

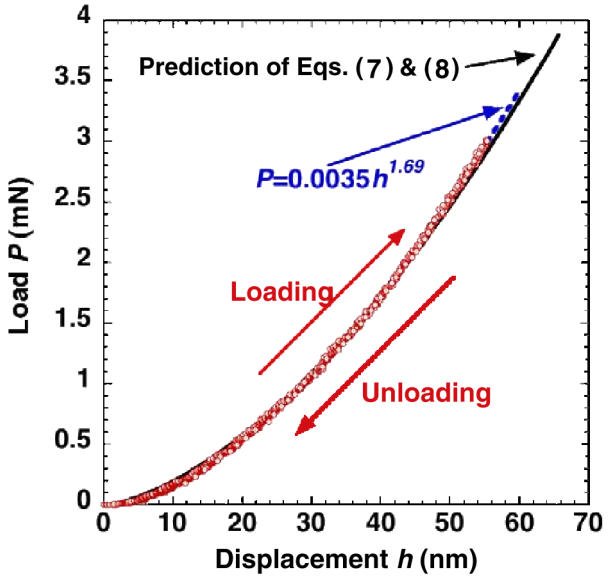

FIG. 3 (color online). Comparison of experimental measurements (circles) to predictions of the elastic load-displacement behavior for a (110) Cr_3Si single crystal below its first pop-in event.

mine the load and displacement relationships for elastic deformation before a pop-in event:

$$P = 2E_r\left\{\frac{aC_2}{4C_1} + \frac{4C_1a^2 - C_2^2}{16C_1\sqrt{C_1}}\left[\frac{\pi}{2} - \arcsin\left(\frac{C_2^2 - 4C_1a^2}{4C_1a^2 + C_2^2}\right)\right]\right\} \tag{7}$$

and

$$h = \frac{a}{2\sqrt{C_1}}\left[\frac{\pi}{2} - \arcsin\left(\frac{C_2^2 - 4C_1a^2}{4C_1a^2 + C_2^2}\right)\right]. \tag{8}$$

For a [110] single crystal of Cr_3Si ($E_r = 293$ GPa) the P-h curve predicted by Eqs. (7) and (8) is compared to experimental data at loads below the pop-in events in Fig. 3. The theoretical P-h curve matches the experimental loading curve remarkably well, thus validating the approach. It should also be noted that the load-displacement data are well described by the power law relation $P = Ch^m$, where $m = 1.69$ (see Fig. 3). The observed exponent, $m = 1.69$, lies between those for spherical and conical indenters ($m = 1.5$ and 2, respectively). This reinforces the notion that, in the depth range of interest, the shape of the Berkovich indenter transitions from spherical to conical and cannot be adequately described by either geometry alone.

Although Sneddon's method can be used to determine the load-displacement relationship, it does not provide for evaluation of the stress field. Schwarzer and Pharr [18] have shown that a mathematical formalism developed by Fabrikant can be useful in evaluating the stresses for an indenter that can be approximated by the power law shape $z = A(r/a)^m$, but the evaluation requires numerical methods that are not straightforward to implement. Instead, elastic finite element simulations were employed here to determine the indentation stress fields and evaluate the maximum resolved shear stresses at the pop-in loads (assuming that Cr_3Si is elastically isotropic with $E_r = 273$ GPa). The accuracy of the finite element simulations was tested by performing computations for a spherical indenter and comparing to the known Hertzian stress field (see, for instance, Johnson [7]). The stresses were found to be within 5% of the Hertzian values.

To resolve the shear stresses onto the (100)[001] slip system, the procedure used by Gerberich *et al.* [5] was employed. Contour plots of the resolved shear stresses at the experimentally observed pop-in loads for three crystallographic orientations are shown in Fig. 4. For purely geometric reasons, the maximum resolved shear stress occurs at a different position beneath the contact surface for each orientation, a point that has not been properly recognized in some previous analyses [3,6]. As shown in Table I, the maximum resolved shear stresses, $\tau_{[100]} = 18.1$ GPa, $\tau_{[110]} = 22.3$ GPa, and $\tau_{[111]} = 21.7$ GPa, are all within 12% of the theoretical shear stress estimated using the relation $\tau_{\text{th}} = G/2\pi = 20.5$ GPa ($G = 129$ GPa [15] for Cr_3Si). The experimental results and analysis are thus consistent with the notion that the first pop-in event corresponds to the nucleation of dislocations when the theoretical shear strength is exceeded.

It is also useful to compare the theoretical strengths evaluated using our new procedure to predictions based on the spherical tip assumption and Hertzian analysis. To do so, we have computed the maximum resolved shear stresses, τ_R, at pop-in events from the Hertzian stress field and include in Table I values for spheres of different radii. The radius $R = 232$ nm is the value consistent with our

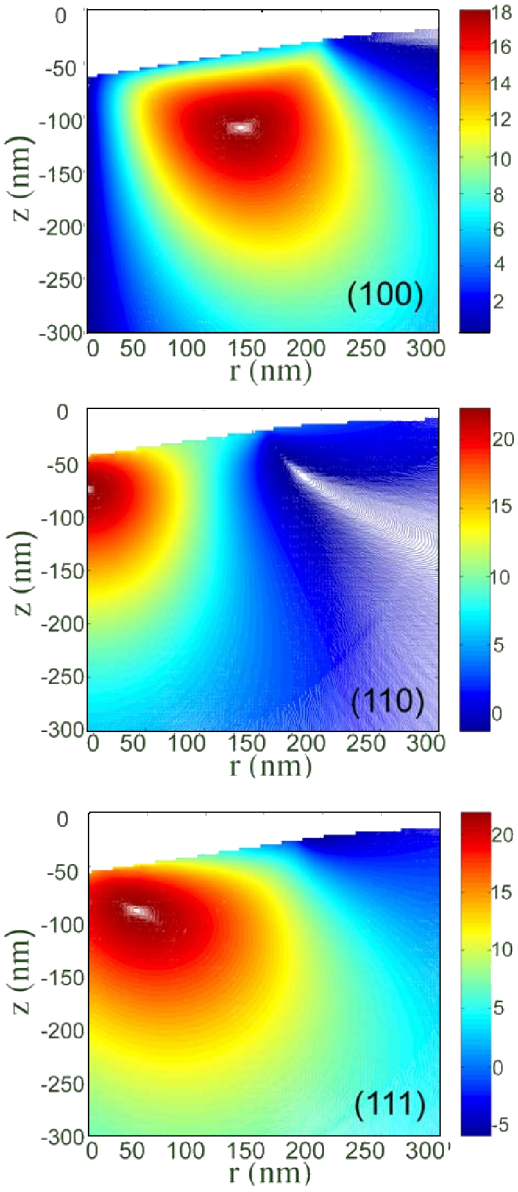

FIG. 4 (color online). Contour plots of resolved shear stress at the pop-in load for three crystallographic orientations in Cr_3Si.

measured area function in the limit of small penetration depth. Another natural value to choose is that derived from analysis of the load-displacement data up to the point of pop-in events assuming Hertzian contact. Using the standard Hertzian relation in Eq. (1), values of the effective tip radius, R_{eff}, derived for the three low-index orientations in Cr_3Si are as follows: [100] $R_{\text{eff}} = 412$ nm; [110] $R_{\text{eff}} = 379$ nm; [111] $R_{\text{eff}} = 358$ nm. The maximum resolved shear stresses based on these values are included in Table I. The value $R = 232$ nm overestimates τ_{max} by as much as 41%. On the other hand, the effective radii, R_{eff}, give more reasonable estimates, suggesting that Hertzian analysis of the P-h data prior to pop-in events is probably the best way to estimate the relevant tip radius.

It should be noted that, although the method developed here is a useful extension of previous analyses that helps to account for potentially important influences of the indenter tip shape, two additional factors may also be important. First, the influences of elastic anisotropy need to be considered in the ways they may influence the stress field. Second, all analyses to date have ignored the fact that there are sharp edges on the indenter. These undoubtedly influence the nature of the stress field, even at the shallowest depths, as evidenced by the observation that images of even the smallest hardness impressions are usually triangular in appearance rather than circular. Small spherical indenters, to the extent they can be obtained and calibrated, would avoid the edge problem in the determination of theoretical strengths from pop-in loads.

This research was sponsored by the Division of Materials Sciences and Engineering, Office of Basic Energy Sciences, U.S. Department of Energy, and the SHaRE Collaborative Research Center at Oak Ridge National Laboratory, under Contract No. DE-AC05-00OR22725 with UT-Battelle, LLC.

[1] W. C. Oliver and G. M. Pharr, J. Mater. Res. **7**, 1564 (1992).
[2] S. Suresh, T. G. Nieh, and B. W. Choi, Scr. Mater. **41**, 951 (1999).
[3] W. Wang, C. B. Jiang, and K. Lu, Acta Mater. **51**, 6169 (2003).
[4] A. Gouldstone, H.-J. Koh, K.-Y. Zeng, A. E. Giannakopoulos, and S. Suresh, Acta Mater. **48**, 2277 (2000).
[5] W. W. Gerberich, J. C. Nelson, E. T. Lilleodden, P. Anderson, and J. T. Wyrobek, Acta Mater. **44**, 3585 (1996).
[6] Y. L. Chiu and A. H. W. Ngan, Acta Mater. **50**, 1599 (2002).
[7] K. L. Johnson, *Contact Mechanics* (Cambridge University Press, Cambridge, England, 1985).
[8] S. G. Corcoran, R. J. Colton, E. T. Lilleodden, and W. W. Gerberich, Phys. Rev. B **55**, R16057 (1997).
[9] T. F. Page, W. C. Oliver, and C. J. McHargue, J. Mater. Res. **7**, 450 (1992).
[10] M. Goken, R. Sakidja, W. D. Nix, and J. H. Perepezko, Mater. Sci. Eng. A **319–321**, 902 (2001).
[11] J. Li, K. J. Van Vliet, T. Zhu, S. Yip, and S. Suresh, Nature (London) **418**, 307 (2002).
[12] J. G. Swadener, I. Rosales, and J. H. Schneibel, Mater. Res. Soc. Symp. Proc. **646**, N4.2 (2001).
[13] C. A. Schuh and T. G. Nieh, Acta Mater. **51**, 87 (2003).
[14] H. Bei, Z. P. Lu, and E. P. George, Phys. Rev. Lett. **93**, 125504 (2004).
[15] H. Bei, E. P. George, and G. M. Pharr, Scr. Mater. **51**, 875 (2004).
[16] G. M. Pharr, W. C. Oliver, and F. R. Brotzen, J. Mater. Res. **7**, 613 (1992).
[17] I. N. Sneddon, Int. J. Eng. Sci. **3**, 47 (1965).
[18] N. Schwarzer and G. M. Pharr, Thin Solid Films **469–470**, 194 (2004).